



Cite this: DOI: 10.1039/d0cy01338b

Efficient photocatalytic oxidative deamination of imine and amine to aldehyde over nitrogen-doped KTi_3NbO_9 under purple light[†]

Zhuobin Yu,^{ab} Xianmo Gu,^{*ac} Ruiyi Wang,^{ac} Jie Wang,^{ac} Jian Zhao,^d
LinJuan Pei^{ac} and Zhanfeng Zheng^{*ac}Received 3rd July 2020,
Accepted 11th August 2020

DOI: 10.1039/d0cy01338b

rsc.li/catalysis

KTi_3NbO_9 nanoparticles were fabricated *via* a simple hydrothermal method with a post-calcination treatment. The nitrogen doping (N- KTi_3NbO_9) leads to a narrow band gap, which in turn facilitates efficiently catalysis of imine deamination under purple light that matches its absorption spectra. Furthermore, N- KTi_3NbO_9 exhibits excellent performance in the tandem reaction of photocatalytic imine formation and deamination from various amines. The conversion of benzylamine was up to 100% with >85% benzaldehyde selectivity.

1 Introduction

The oxidative deamination reactions are widely applied for the generation of diverse reactive intermediates in organic syntheses.¹ For example, the deamination of aromatic amines is an important method for the conversion of imino groups to aldehydes or ketones, which are critical intermediates in the synthesis of amino acids, adenine, guanine, cytosine, and their derivatives, as shown in Scheme 1.^{2,3} At present, the deamination of aromatic amines is mainly achieved *via* an indirect pathway involving aryl diazonium salt intermediates (Sandmeyer reaction or Meerwein reaction), which requires harsh experimental conditions.^{4,5} Therefore, the selective transformation of aromatic amines under mild conditions has attracted considerable attention.^{6,7} The utilization of solar energy to drive this chemical transformation is a promising approach in the context of green and sustainable chemistry.⁸

Numerous catalysts, such as TiO_2 and Nb_2O_5 , have been explored during the past few years for such a photocatalytic chemical transformation. These works mainly focus on the oxidative coupling of amines.^{9–13} There are few reports on photocatalytic amine deamination, a tandem reaction of amine oxidative coupling, and deamination of imines. KTi_3NbO_9 ,

shown in Fig. S1,[†] is considered as a promising photocatalyst due to its unique tunnel structure.^{14–16} Moreover, nitrogen-doped KTi_3NbO_9 (N- KTi_3NbO_9) showed significantly improved optical properties (electronic structure), endowing it with advantageous electrical conductivity and thermal stability.^{17,18} In this study, KTi_3NbO_9 nanoparticles were obtained *via* a hydrothermal method, followed by post-calcination. N- KTi_3NbO_9 photocatalysts were then fabricated by annealing KTi_3NbO_9 under ammonia gas (NH_3). The doped catalyst showed excellent performance in photocatalytic imine deamination and the tandem reaction of amine oxidative coupling and imine deamination under purple light irradiation. We also found that the high conversion of amines with high deamination efficiency was achieved when the light source matched with the light absorption properties of N- KTi_3NbO_9 .

2 Experimental

2.1 Photocatalysts preparation

All chemicals were purchased from Sinopharm Chemical Reagent Co., Ltd., and used without further purification. KTi_3NbO_9 (abbreviated as KTNO) was prepared *via* a hydrothermal process with post-sintering. Briefly, niobium oxalate [$\text{Nb}(\text{HC}_2\text{O}_4)_5$, 1.61 g] and titanium oxysulfate ($\text{TiOSO}_4 \cdot x\text{H}_2\text{O}$, 1.72 g) were added to an aqueous KOH

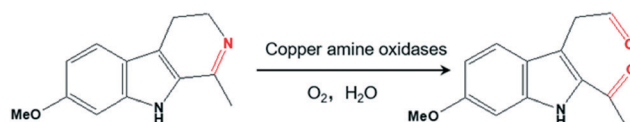
^a State Key Laboratory of Coal Conversion, Institute of Coal Chemistry, Chinese Academy of Sciences, Taiyuan 030001, Shanxi, China. E-mail: zfzheng@sxicc.ac.cn, guxm@sxicc.ac.cn

^b Taiyuan University of Technology, Taiyuan 030024, China

^c Center of Materials Science and Optoelectronics Engineering, University of Chinese Academy of Sciences, Beijing, 100049, China

^d Tianjin Key Laboratory of Organic Solar Cells and Photochemical Conversion, School of Chemistry and Chemical Engineering, Tianjin University of Technology, Tianjin, 300384, China

[†] Electronic supplementary information (ESI) available. See DOI: 10.1039/d0cy01338b



Scheme 1 An example of oxidative deamination reactions available.³

solution (1 M, 50 mL), and the mixture was stirred for 1 h. This solution was then transferred to a PTFE-lined autoclave (100 mL in volume) and kept at 180 °C for 24 h. After the hydrothermal process, the white precipitate was separated *via* centrifugation, washed with deionized water, and dried in air for 12 h at 80 °C, respectively. The final KTNO nanoparticles were obtained by calcining the dried precipitate for 2 h at 900 °C under air atmosphere. Similarly, N-KTi₃NbO₉ (abbreviated as N-KTNO) nanoparticles were obtained by calcining the dried precipitate for 2 h at 900 °C under an NH₃ atmosphere, followed by treatment in air at 500 °C. The optimized calcination time for N-KTNO in air was determined by the photocatalytic activity (Fig. S2†). For comparison, g-C₃N₄ was prepared according to literature.¹⁹

2.2 Characterization

X-ray diffraction (XRD) patterns were acquired using a MiniFlex II diffractometer employing Cu K_α radiation ($\lambda = 1.5418 \text{ \AA}$). A 2100F transmission electron microscope operated at 200 kV was used, with an attachment for energy-dispersive spectroscopy (EDS). Nitrogen sorption isotherms were recorded on an automatic adsorption instrument (Micromeritics, TriStar II 3020 analyzer), operating at the liquid nitrogen temperature (77 K). UV-vis diffuse-reflectance (UV-vis-DR) spectra were recorded on a Shimadzu UV-3600 spectrophotometer. X-ray photoelectron spectra (XPS) were recorded on a Thermo ESCALAB 250 spectrometer, employing an Al K_α X-ray source ($h\nu = 1486.6 \text{ eV}$). Binding energies were calibrated with respect to the C1s peak at 284.6 eV. Photoluminescence (PL) spectra were recorded on a Hitachi F-7000 FL spectrophotometer. The photoelectrochemical measurements were studied on an electrochemical station (CHI660E, Chenhua, China). The electron paramagnetic resonance (EPR) spectra were recorded using a Bruker EMXPLUS10/12 EPR electron paramagnetic resonance spectrometer.

2.3 Photocatalytic activity test

Typically, the photocatalytic activity for selective amine or imine oxidation was conducted under the irradiation of a 100 W COB LED lamp at 80 °C in an air-tight flask sealed with 1 atm of O₂ (flushed with 0.35 mL s⁻¹ of O₂ flow for 1 min prior to use). The reaction mixture consists of benzylamine (0.08 mmol) or *N*-benzylidenebenzylamine (0.04 mmol), photocatalyst (20 mg), and acetonitrile (2 mL) as the solvent. The obtained product was analyzed *via* GC (Shimadzu 2014C GC; WondaCap 5 column) and GC-MS (Bruker SCION SQ 456). The output spectra of various colored LEDs, namely a purple LED (375–430 nm, maximum at 400 nm), a blue LED (425–510 nm, maximum at 455 nm), green LED (475–600 nm, maximum at 525 nm), are presented in Fig. S3.†

3 Results and discussions

3.1 Physicochemical properties of KTNO and N-KTNO

The powder XRD patterns of the prepared KTNO and N-KTNO are presented in Fig. 1a, and are in agreement with those of orthorhombic KTi₃NbO₉ (space group *C2/m*, lattice parameters $a = 6.392 \text{ \AA}$, $b = 3.785 \text{ \AA}$, $c = 14.865 \text{ \AA}$) (JCPDS No. 17-0312). Notably, the XRD pattern of KTNO is similar to that of N-KTNO, which demonstrates that nitrogen doping does not change lattice nor phase structure. Fig. 1b shows TEM images and HR-TEM analysis of the prepared KTNO and N-KTNO. The mean diameter of the KTNO nanoparticles is 80 nm. Lattice distance was 0.32 and 0.30 nm, corresponding to the (200) and (112) planes of KTi₃NbO₉. Similar mean particle diameter and lattice distance were also observed for N-KTNO. The specific surface areas for KTNO and N-KTNO are small at 2.08 and 6.20 m² g⁻¹, respectively (Fig. S4†).

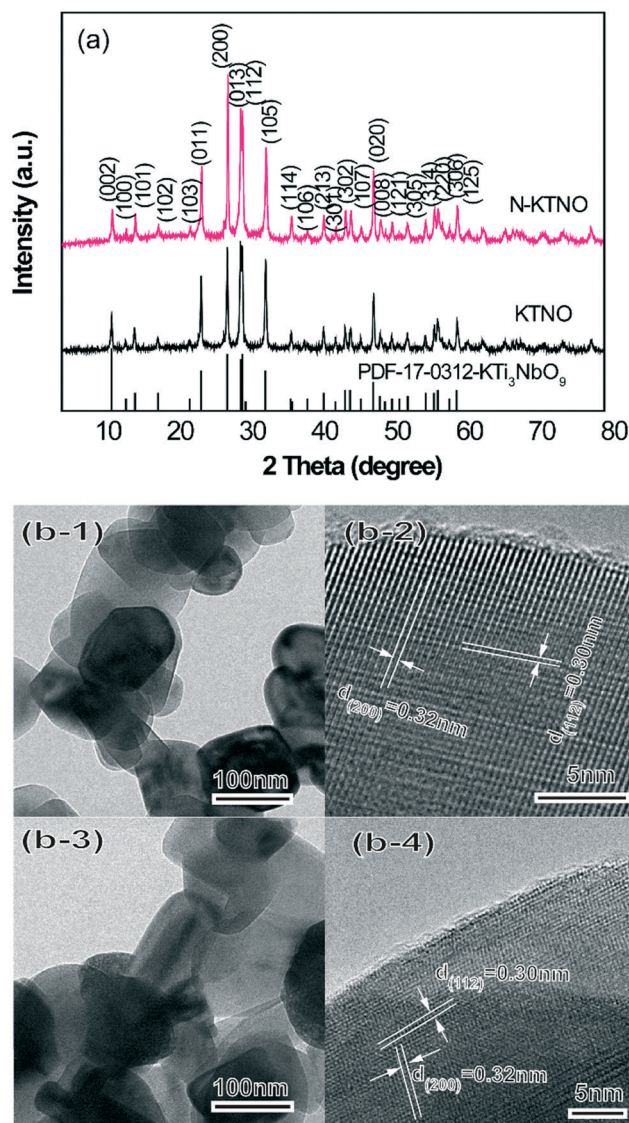


Fig. 1 (a) XRD patterns of KTNO and N-KTNO, (b) TEM images and HRTEM analysis of KTNO (b-1 and b-2), and N-KTNO (b-3 and b-4).

The XPS spectra of KTNO and N-KTNO are shown in Fig. S5.† K 2p_{3/2} and K 2p_{1/2} peaks at 292.2 and 294.8 eV can be assigned to K⁺ in the titanate.²⁰ Ti 2p_{3/2} and Ti 2p_{1/2} peaks at 458.0 and 464.0 eV are ascribed to Ti⁴⁺, and Nb 3d_{5/2} and Nb 3d_{3/2} peaks at 206.3 and 209.0 eV can be ascribed to Nb⁵⁺.^{21,22} O 1s peaks at 529.5 and 532.0 eV are attributed to O–M and O–H species, respectively.²³ The K 2p, Ti 2p, Nb 3d, and O 1s peaks of N-KTNO are the same as KTNO. Additionally, characteristic N 1s peaks are observed at 395.7 and 399.7 eV for N–M (M = Ti or Nb) or molecularly chemisorbed nitrogen,^{24,25} which indicates that N is doped into KTNO successfully. The N content in N-KTNO was estimated to be 0.84 at%.

The colour of KTNO changes from white to greyish-green after N-doping (Fig. 2a), resulting in extended absorption in the visible-light range.²⁶ The extended absorption is confirmed by the UV-vis-DR spectra in Fig. 2a. The absorption edge of KTNO was approx. at 430 nm, while it obviously red-shifted to approx. 500 nm after N-doping. Based on the UV-vis-DR spectra and $E_g = 1240/\lambda$ (λ , the cut-off wavelength), the band gap E_g of KTNO and N-KTNO

photocatalysts are 2.88 and 2.45 eV, respectively.²² In Fig. 2b, both KTNO and N-KTNO are n-type semiconductors, and the flat band potentials (namely Fermi energy level, E_f) are 0.43 eV (KTNO) and 0.47 eV (N-KTNO) vs. Ag/AgCl, which are respectively 0.17 eV and 0.13 eV vs. RHE for KTNO and N-KTNO according to literature.^{27,28} Moreover, as shown in Fig. 2c, the relative potential of the valance band (VB) vs. the Fermi energy level was 1.39 eV for KTNO and 0.96 eV for N-KTNO, respectively. Consequently, we plotted their band alignment in Fig. 2d. The change in the bandgap structure was caused by a new N 2p orbital formed above the O 2p VB after N-doping.²⁹ Fig. S6† shows the PL spectra of KTNO and N-KTNO. The peaks at 540 and 630 nm are ascribed to TiO₆ units and the defect-related energy, respectively.^{30,31} Compared with KTNO, the PL intensity of N-KTNO decreased significantly. In Fig. S7(a),† it can be observed that the photocurrent response of N-KTNO is remarkably improved. Furthermore, in Fig. S7(b),† it is apparently found that the arc radius of N-KTNO is obviously smaller than that of KTNO, indicating that N-KTNO can efficiently promote the transportation of photo-generated charge carriers at the

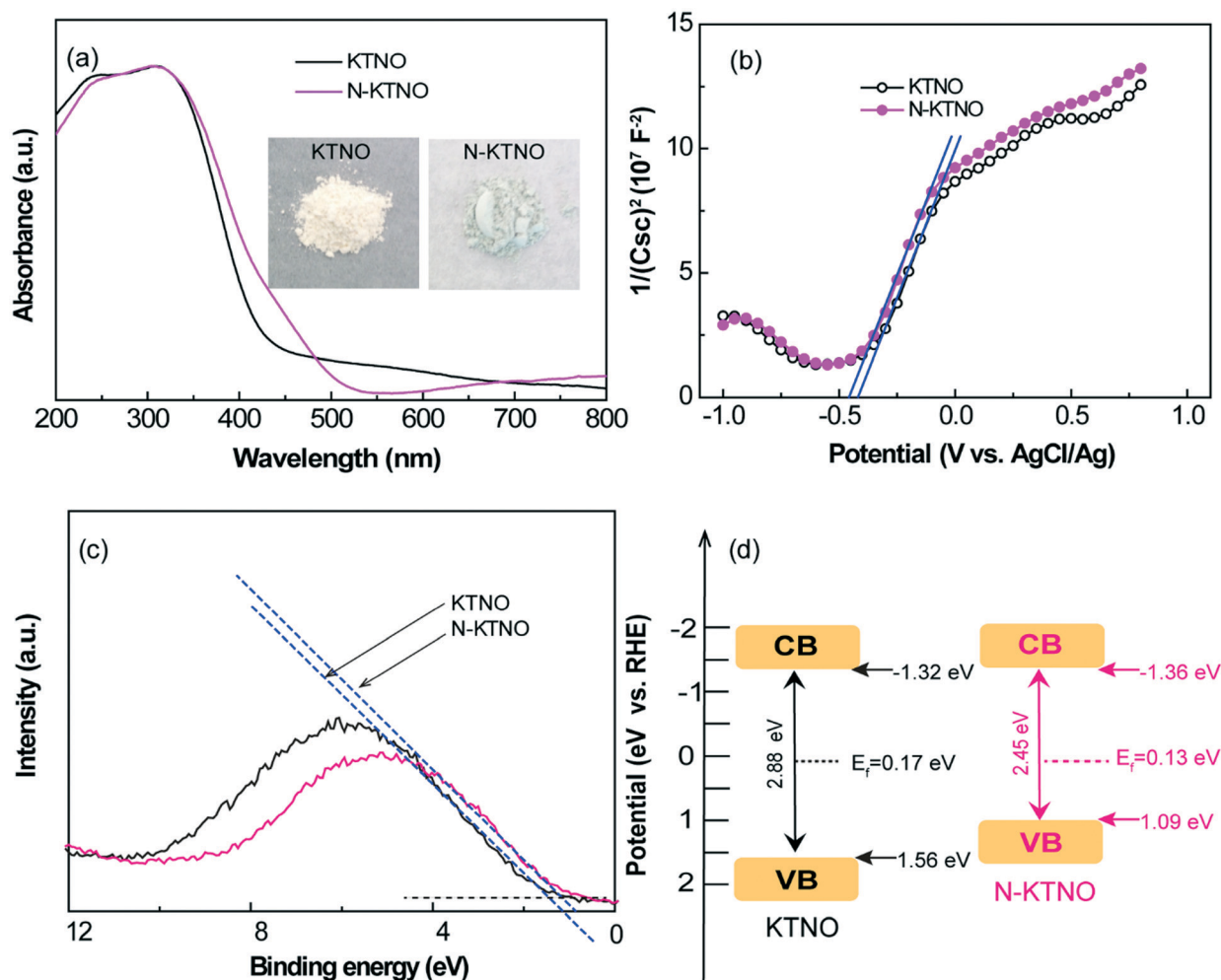


Fig. 2 (a) Electronic photographs and UV-vis-DR spectra, (b) Mott-Schottky curves, (c) valence-band XPS spectra and (d) the schematic diagram of the DOS of KTNO and N-KTNO.

material surface/interface. Consequently, in combination with the above results, this implies that N-doping enhances the charge separation and photocatalytic performance of KTNO.

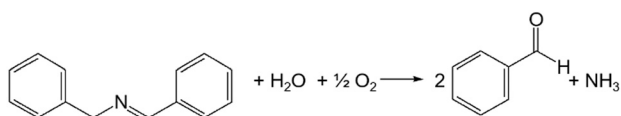
3.2 Photocatalytic activity for imine (*N*-benzylidenebenzylamine) deamination over N-KTNO under purple light

The photocatalytic performances of N-KTNO for imine deamination (selective aerobic oxidation of *N*-benzylidenebenzylamine) (Scheme 2) under white and single-colored (purple, blue, and green) LED illumination are shown in Fig. 3a. The activity does not change much when the catalyst amount is more than 20 mg (Fig. S8†). Therefore, 20 mg of catalyst was applied in this study to eliminate the surface area difference. The conversion rate of imine was respectively 25.1% and 18.8% with a high benzaldehyde selectivity (87.0% and 93.1%) for white and blue light, whereas it decreases to 3.5% under green light. Under purple light irradiation, the conversion rate exceeds 95% with >80% selectivity for benzaldehyde, accompanied by a trace of PhCH=NH, as identified by GC-MS (Fig. S9†). Then, the time-course of imine conversion and benzaldehyde generated under purple light irradiation was studied, as given in Fig. 3b. The imine conversion rate increases linearly from 35.2% to 97.0% with a high benzaldehyde selectivity as prolonging the reaction time. The rest of the products contained benzamide (3.8%), *N*-formylbenzylamine (6.8%) and other impurities with trace amounts.

For comparison, traditional photocatalysts P25 and g-C₃N₄ were also utilized in *N*-benzylidenebenzylamine deamination under purple light irradiation. In Fig. 3c, N-KTNO, P25 and g-C₃N₄ showed excellent imine conversion, superior to KTNO. However, the benzaldehyde selectivity for P25 and g-C₃N₄ was much lower than that for N-KTNO. The benzaldehyde yield was in the order of N-KTNO > P25 > g-C₃N₄ > KTNO. These results demonstrated that N-KTNO exhibits excellent performance in photocatalytic imine deamination.³² The stability of the N-KTNO photocatalyst for imine deamination is presented in Fig. S10,† where N-KTNO seems to be a highly efficient and robust photocatalyst for the described process in terms of the conversion rate of imine and the selectivity for benzaldehyde.

3.3 Proposed photocatalytic imine (*N*-benzylidenebenzylamine) deamination mechanism

The mechanism of the photocatalytic imine deamination under purple light was investigated. The absorption edge of



Scheme 2 The reaction formula for imine deamination (selective aerobic oxidation imine).

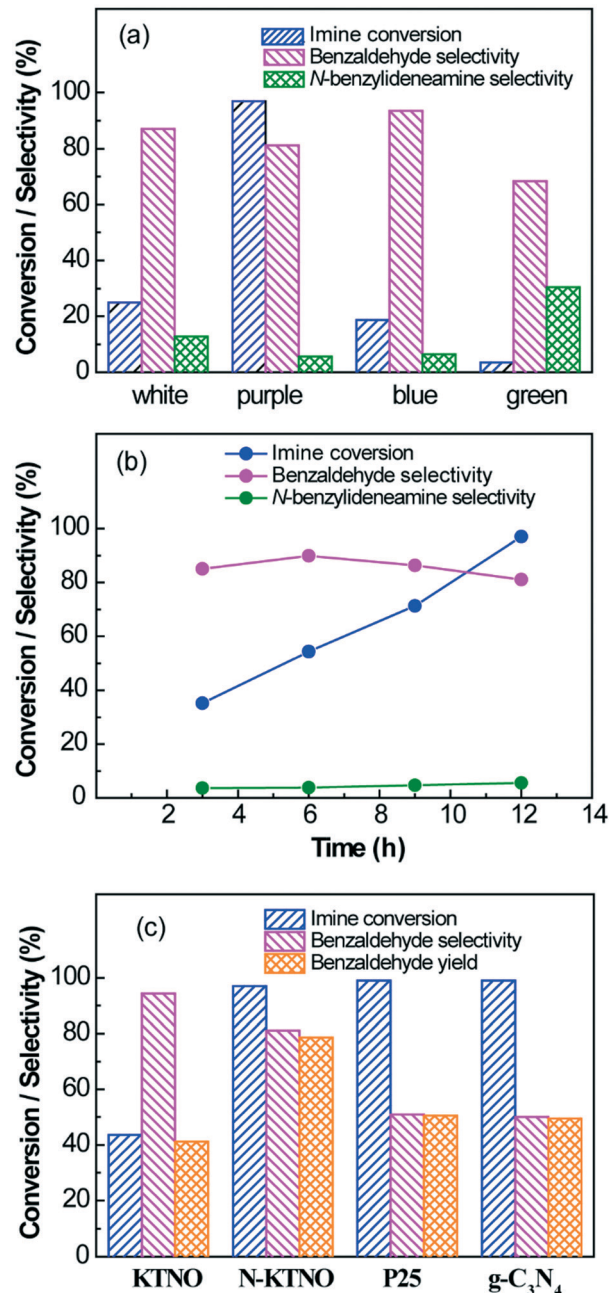


Fig. 3 (a) Imine conversion, benzaldehyde selectivity under white and single-colored LED lights, (b) the time profile for *N*-benzylidenebenzylamine deamination under purple light, (c) imine conversion and benzaldehyde selectivity over different samples under purple light. Light intensity 200 mW cm⁻², 80 °C, 12 h.

N-KTNO before and after *N*-benzylidenebenzylamine adsorption was located at 500 and 530 nm, respectively. The absorption difference also led to the formation of a new band centered at 410 (Fig. S11†). These results imply that a new surface complex is probably formed between the adsorbed *N*-benzylidenebenzylamine and N-KTNO. The absorption band of this surface complex matches well with the light spectrum of purple LED lights (inset, Fig. 4). Moreover, as stated above, the highest photocatalytic activity was achieved

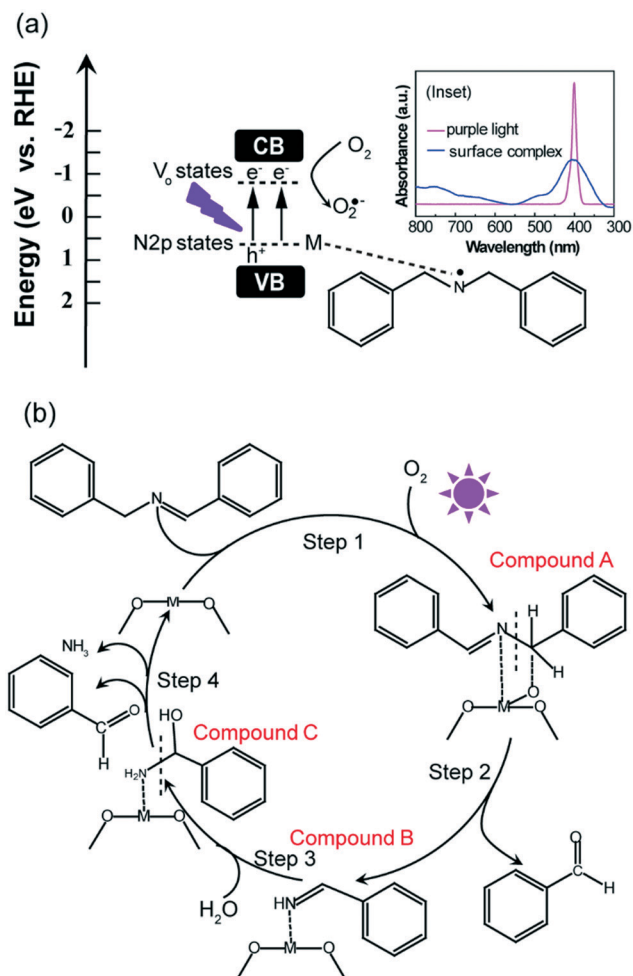


Fig. 4 (a) Schematic of adsorbed *N*-benzylidenebenzylamine and *N*-KTNO photocatalyst; (inset) the light spectrum of purple LED lights and surface complex; (b) proposed mechanism for imine deamination (selective aerobic oxidation of *N*-benzylidenebenzylamine to benzaldehyde) over the *N*-KTNO photocatalyst under purple light irradiation.

for the purple light. Thus, we proposed that the surface complex could absorb light and participate in a direct electron transfer from a donor level, which consists of N 2p orbitals from both the adsorbed amine species and CB of *N*-KTNO (Fig. 4a). A plausible mechanism is shown in Fig. 4b.

In step 1, the surface complex (amide species) was formed between the *N*-benzylidenebenzylamine reactant and *N*-KTNO photocatalyst. Under purple light irradiation, the surface complex absorbs light and initiates the reaction by generating holes and electrons (Fig. 4a). Photo-generated electrons could be captured by O_2 forming $O_2^{\cdot-}$. The resulting radicals will react with the amide species to produce compound A. In step 2, the deamination product benzaldehyde and $PhCH=NH$ intermediate were obtained by the C–N bond cleavage of compound A. The $PhCH=NH$ intermediate adsorbs on the surface of *N*-KTNO (compound B). In step 3, the adsorbed $PhCH=NH$ intermediate is attacked by H_2O forming another benzaldehyde product *via* compound C. The final step would

be the NH_3 desorption from the catalyst surface. Then, the active sites return to the original state for another reaction cycle.

3.4 Photocatalytic activity for the tandem reaction of imine formation and deamination over *N*-KTNO under purple light

As mentioned in the introduction, great efforts have been made towards the development of photocatalysts for the oxidative coupling of amines to imines, such as Nb_2O_5 (ref. 13, 33 and 34) and TiO_2 .^{35,36} If the same process could be driven by *N*-KTNO, it is possible to photocatalyze the selective one-pot oxidation of primary amines to aldehydes *via* imine intermediates, thereby succeeding in the photocatalytic tandem reaction of imine formation and imine deamination under mild conditions.⁷ As shown in Fig. 5, the conversion rate of benzylamine to corresponding imine (>85% selectivity) increases as the reaction time prolongs to 5 h. A trace amount of benzaldehyde was detected as an intermediate during the formation of the imine, which is consistent with previous reports.^{33,35–38} After 5 h, the selectivity for benzaldehyde products rapidly increases, accompanied by a dramatic decrease of imine selectivity. The final benzaldehyde product selectivity was up to 90% with 100% benzylamine conversion. These results indicate that the tandem reaction of benzylamine oxidative coupling and imine deamination could be successfully driven by *N*-KTNO in one-pot photocatalytic reactions.

Photocatalytic of the tandem reaction of benzylamine oxidative coupling and imine deamination over various photocatalysts are summarized in Table S1.† The conversion of benzylamine over *N*-KTNO far exceeds KTNO, which can be attributed to two aspects: (1) the narrow bandgap of *N*-KTNO (Fig. 2), which efficiently improve light utilization, and (2) abundant oxygen vacancies, which facilitate the adsorption of water (Scheme 2) and the formation of

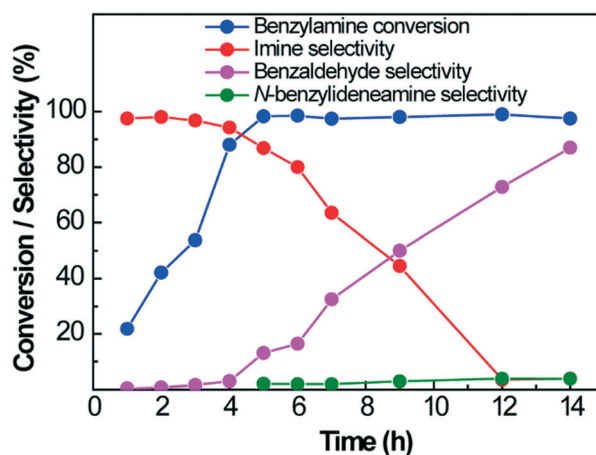


Fig. 5 The time profile for the tandem reaction of benzylamine deamination. Reaction conditions: *N*-KTNO catalyst (20 mg), benzylamine (0.08 mmol), acetonitrile (2 mL), purple light 200 mW cm^{-2} , 80 °C.

benzaldehyde.³⁹ The analysis for the number of oxygen vacancies is provided in Fig. S12.† Moreover, the yield of the benzaldehyde product over N-KTNO (1210 mmol mol_{catalyst}⁻¹) is also much higher than those over TiO₂ (197 mmol mol_{catalyst}⁻¹) and Nb₂O₅ (430 mmol mol_{catalyst}⁻¹). In addition, N-KTNO achieves a much higher catalytic activity than other thermal catalysts reported in terms of benzaldehyde yield, reaction time and temperature (Table S2†).^{7,39,40}

To further demonstrate the extensive application of N-KTNO in this tandem reaction, various amines were examined (Table S3†). The high conversion of different amines with high efficiency of imines deamination to aldehyde products is achieved (Table S3,† entries 1–5). The results in Table S3† also confirm that aldehyde formation is *via* the deamination of corresponding imine intermediates. However, the photocatalytic activity is low when utilizing phenylethylamine as a reactant (Table S2,† entry 6). These results imply that the presence of an *N*-benzyl group plays a crucial role in imine deamination, which may be responsible for stabilizing the adjacent –C.³⁵

4 Conclusions

In summary, N-KTi₃NbO₉ nanoparticles are obtained *via* a simple hydrothermal method, followed by a post-calcination treatment. The N-KTi₃NbO₉ photocatalyst was fabricated by annealing KTNO under NH₃ and air atmosphere in sequence. N-KTi₃NbO₉ achieves excellent photocatalytic activity in imine deamination under the light matched with its absorption properties. Moreover, N-KTi₃NbO₉ shows outstanding photocatalytic performance for the selective aerobic oxidation of amines to aldehydes *via* imine intermediates, and this may give crucial insights for the mechanism investigation in amines oxidative coupling reactions. In this study, the tandem reaction of imine formation and deamination, or the transformation from aromatic amine to aromatic imine, and then to aromatic aldehyde under mild conditions in one-pot was successfully achieved. We believe that this synthetic strategy is practicable and can be extended to diverse photocatalytic reactions.

Conflicts of interest

There are no conflicts to declare.

Acknowledgements

We appreciate the financial support from the National Natural Science Foundation of China (No. 21773284) and the Hundred Talents Program of the Chinese Academy of Sciences and Shanxi Province.

Notes and references

- 1 S. Ghosh and C. Jana, Metal free biomimetic deaminative direct C-C coupling of unprotected primary amines with active methylene compounds, *Org. Biomol. Chem.*, 2019, **17**(48), 10153–10157.

- 2 B. Chen, L. Wang and S. Gao, Recent advances in aerobic oxidation of alcohols and amines to imines, *ACS Catal.*, 2015, **5**(10), 5851–5876.
- 3 T. Nagakubo, T. Kumano, T. Ohta, Y. Hashimoto and M. Kobayashi, Copper amine oxidases catalyze the oxidative deamination and hydrolysis of cyclic imines, *Nat. Commun.*, 2019, **10**(1), 413–424.
- 4 L. Liu and J. Zhang, Gold-catalyzed transformations of alpha-diazocarbonyl compounds: selectivity and diversity, *Chem. Soc. Rev.*, 2016, **45**(3), 506–516.
- 5 B. Ma, Z. Wu, B. Huang, L. Liu and J. Zhang, Gold-catalysed facile access to indene scaffolds via sequential C-H functionalization and 5-endo-dig carbocyclization, *Chem. Commun.*, 2016, **52**(60), 9351–9354.
- 6 Q. Xiao, T. Connell, J. Cadusch, A. Roberts, A. Chesman and D. Gomez, Hot-carrier organic synthesis via the near-perfect absorption of light, *ACS Catal.*, 2018, **8**(11), 10331–10339.
- 7 G. Golime, G. Bogonda, H. Kim and K. Oh, Biomimetic oxidative deamination catalysis via ortho-naphthoquinone-catalyzed aerobic oxidation strategy, *ACS Catal.*, 2018, **8**(6), 4986–4990.
- 8 D. Cambie, C. Bottecchia, N. Straathof, V. Hessel and T. Noel, Applications of continuous-flow photochemistry in organic synthesis, material science, and water treatment, *Chem. Rev.*, 2016, **116**(17), 10276–10341.
- 9 Z. Yu, E. Waclawik, Z. Wang, X. Gu, Y. Yuan and Z. Zheng, Dual modification of TiNb₂O₇ with nitrogen dopants and oxygen vacancies for selective aerobic oxidation of benzylamine to imine under green light, *J. Mater. Chem. A*, 2017, **5**(9), 4607–4615.
- 10 X. Lang, H. Ji, C. Chen, W. Ma and J. Zhao, Selective formation of imines by aerobic photocatalytic oxidation of amines on TiO₂, *Angew. Chem., Int. Ed.*, 2011, **50**(17), 3934–3937.
- 11 X. Lang, W. Ma, Y. Zhao, C. Chen, H. Ji and J. Zhao, Visible-light-induced selective photocatalytic aerobic oxidation of amines into imines on TiO₂, *Chem. – Eur. J.*, 2012, **18**(9), 2624–2631.
- 12 S. Furukawa, Y. Ohno, T. Shishido, K. Teramura and T. Tanaka, Selective amine oxidation using Nb₂O₅ photocatalyst and O₂, *ACS Catal.*, 2011, **1**(10), 1150–1153.
- 13 Y. Zhang, L. Pei, Z. Zheng, Y. Yuan, T. Xie and J. Yang, *et al.*, Heterojunctions between amorphous and crystalline niobium oxide with enhanced photoactivity for selective aerobic oxidation of benzylamine to imine under visible light, *J. Mater. Chem. A*, 2015, **3**(35), 18045–18052.
- 14 A. Wadsley, Alkali titanoniobates - crystal structures of KTiNbO₅ + KTi₃NbO₉, *Acta Crystallogr.*, 1964, **17**(6), 623–625.
- 15 K. Teshima, S. Lee, A. Yamaguchi, S. Suzuki, K. Yubuta and T. Ishizaki, *et al.*, The growth of highly crystalline, idiomorphic potassium titanoniobate crystals by the cooling of a potassium chloride flux, *CrystEngComm*, 2011, **13**(4), 1190–1196.
- 16 J. Colin, V. Pralong, M. Hervieu, V. Caignaert and B. Raveau, Lithium insertion in an oriented nanoporous oxide with a tunnel structure: Ti₂Nb₂O₉, *Chem. Mater.*, 2008, **20**(4), 1534–1540.

- 17 M. Yang, A. VanWassen, R. Guarecuco, H. Abruna and F. DiSalvo, Nano-structured ternary niobium titanium nitrides as durable non-carbon supports for oxygen reduction reaction, *Chem. Commun.*, 2013, **49**(92), 10853–10855.
- 18 S. Dong, X. Chen, X. Zhang and G. Cui, Nanostructured transition metal nitrides for energy storage and fuel cells, *Coord. Chem. Rev.*, 2013, **257**(13–14), 1946–1956.
- 19 L. Ge, C. Han, X. Xiao and L. Guo, In situ synthesis of cobalt-phosphate (Co-Pi) modified g-C₃N₄ photocatalysts with enhanced photocatalytic activities, *Appl. Catal., B*, 2013, **142**, 414–422.
- 20 D. Salinas, S. Guerrero, A. Cross, P. Araya and E. Wolf, Potassium titanate for the production of biodiesel, *Fuel*, 2016, **166**, 237–244.
- 21 L. Kong, Z. Jiang, C. Wang, F. Wan, Y. Li and L. Wu, *et al.*, Simple ethanol impregnation treatment can enhance photocatalytic activity of TiO₂ nanoparticles under visible-light irradiation, *ACS Appl. Mater. Interfaces*, 2015, **7**(14), 7752–7758.
- 22 H. Huang, C. Wang, J. Huang, X. Wang, Y. Du and P. Yang, Structure inherited synthesis of N-doped highly ordered mesoporous Nb₂O₅ as robust catalysts for improved visible light photoactivity, *Nanoscale*, 2014, **6**(13), 7274–7280.
- 23 S. Lou, Y. Ma, X. Cheng, J. Gao, Y. Gao and P. Zuo, *et al.*, Facile synthesis of nanostructured TiNb₂O₇ anode materials with superior performance for high-rate lithium ion batteries, *Chem. Commun.*, 2015, **51**(97), 17293–17296.
- 24 J. Yuan, M. Chen, J. Shi and W. Shangguan, Preparations and photocatalytic hydrogen evolution of N-doped TiO₂ from urea and titanium tetrachloride, *Int. J. Hydrogen Energy*, 2006, **31**(10), 1326–1331.
- 25 Z. Zhai, Y. Huang, L. Xu, X. Yang, C. Hu and L. Zhang, *et al.*, Thermostable nitrogen-doped HTiNbO₅ nanosheets with a high visible-light photocatalytic activity, *Nano Res.*, 2011, **4**(7), 635–647.
- 26 H. Park, H. Wu, T. Song, X. David Lou and U. Paik, Porosity-Controlled TiNb₂O₇ microspheres with partial nitridation as a practical negative electrode for high-power Lithium-Ion batteries, *Adv. Energy Mater.*, 2015, **5**(8), 1401945.
- 27 C. Yao, R. Wang, Z. Wang, H. Lei, X. Dong and C. He, Highly dispersive and stable Fe³⁺ active sites on 2D graphitic carbon nitride nanosheets for efficient visible-light photocatalytic nitrogen fixation, *J. Mater. Chem. A*, 2019, **7**(48), 27547–27559.
- 28 C. Yao, A. Yuan, Z. Wang, H. Lei, L. Zhang and L. Guo, *et al.*, Amphiphilic two-dimensional graphitic carbon nitride nanosheets for visible-light-driven phase-boundary photocatalysis, *J. Mater. Chem. A*, 2019, **7**(21), 13071–13079.
- 29 H. Park, T. Song and U. Paik, Porous TiNb₂O₇ nanofibers decorated with conductive Ti_{1-x}Nb_xN bumps as a high power anode material for Li-ion batteries, *J. Mater. Chem. A*, 2015, **3**(16), 8590–8596.
- 30 A. Kudo and E. Kaneko, Photoluminescent properties of ion-exchangeable layered oxides, *Microporous Mesoporous Mater.*, 1998, **21**(4–6), 615–620.
- 31 Q. Ma, Y. Zhou, M. Lu, A. Zhang and G. Zhou, Synthesis and luminescence of pure and Eu³⁺-activated Aurivillius-type Bi₃-TiNbO₉ nanophosphors, *Mater. Chem. Phys.*, 2009, **116**(2–3), 315–318.
- 32 G. Liu, L. Wang, C. Sun, X. Yan, X. Wang and Z. Chen, *et al.*, Band-to-band visible-light photon excitation and photoactivity induced by homogeneous nitrogen doping in layered titanates, *Chem. Mater.*, 2009, **21**(7), 1266–1274.
- 33 S. Furukawa, Y. Ohno, T. Shishido, K. Teramura and T. Tanaka, Selective amine oxidation using Nb₂O₅ photocatalyst and O₂, *ACS Catal.*, 2011, **1**(10), 1150–1153.
- 34 S. Furukawa, Y. Ohno, T. Shishido, K. Teramura and T. Tanaka, Reaction mechanism of selective photooxidation of amines over Niobium Oxide: visible-light-induced electron transfer between adsorbed amine and Nb₂O₅, *J. Phys. Chem. C*, 2013, **117**(1), 442–450.
- 35 X. Lang, W. Ma, Y. Zhao, C. Chen, H. Ji and J. Zhao, Visible-light-induced selective photocatalytic aerobic oxidation of amines into imines on TiO₂, *Chemistry*, 2012, **18**(9), 2624–2631.
- 36 X. Lang, H. Ji, C. Chen, W. Ma and J. Zhao, Selective formation of imines by aerobic photocatalytic oxidation of amines on TiO₂, *Angew. Chem., Int. Ed.*, 2011, **50**(17), 3934–3937.
- 37 L. Aschwanden, T. Mallat, M. Maciejewski, F. Krumeich and A. Baiker, Development of a new generation of gold catalysts for amine oxidation, *ChemCatChem*, 2010, **2**(6), 666–673.
- 38 B. Zhu, M. Lazar, B. Trewyn and R. Angelici, Aerobic oxidation of amines to imines catalyzed by bulk gold powder and by alumina-supported gold, *J. Catal.*, 2008, **260**(1), 1–6.
- 39 L. Al-Hmoud and C. Jones, Reaction pathways over copper and cerium oxide catalysts for direct synthesis of imines from amines under aerobic conditions, *J. Catal.*, 2013, **301**, 116–124.
- 40 L. Gong, L. Xing, T. Xu, X. Zhu, W. Zhou and N. Kang, *et al.*, Metal-free oxidative olefination of primary amines with benzylic C-H bonds through direct deamination and C-H bond activation, *Org. Biomol. Chem.*, 2014, **12**(34), 6557–6560.